LUBRICATION OF POLYSILICON MICROMECHANISMS WITH SELF-ASSEMBLED MONOLAYERS

Uthara Srinivasan, Jonathan D. Foster*, Usman Habib, Roger T. Howe, and Roya Maboudian**
Departments of Chemical Engineering, Applied Science & Technology*
and Electrical Engineering & Computer Science**
Berkeley Sensor and Actuator Center
Berkeley, CA 94720-1774

Donna Cowell Senft and Michael T. Dugger
Sandia National Laboratories
PO Box 5800, MS 0340
Albuquerque, NM 87185-0340

ABSTRACT

Here, we report on the lubricating effects of self-assembled monolayers (SAMs) on MEMS by measuring static and dynamic friction with two polysilicon surface-micromachined devices. The first test structure is used to study friction between laterally sliding surfaces and with the second, friction between vertical sidewalls can be investigated. Both devices are SAM-coated following the sacrificial oxide etch and the microstructures emerge released and dry from the final water rinse. The coefficient of static friction, μ_s, was found to decrease from 2.1 ± 0.8 for the SiO_2 coating to 0.11 ± 0.01 and 0.10 ± 0.01 for films derived from octadecyltrichloro-silane (OTS) and 1H,1H,2H,2H-perfluorodecyltrichlorosilane (FDTS). Both OTS and FDTS SAM-coated structures exhibit dynamic coefficients of friction, μ_d, of 0.08 ± 0.01. These values were found to be independent of the apparent contact area, and remain unchanged after 1 million impacts at 5.6 μN (17 kPa), indicating that these SAMs continue to act as boundary lubricants despite repeated impacts. Measurements during sliding friction from the sidewall friction testing structure give comparable initial μ_d values of 0.02 at a contact pressure of 84 MPa. After 15 million wear cycles, μ_d was found to rise to 0.27. Wear of the contacting surfaces was examined by SEM. Standard deviations in the μ data for SAM treatments indicate uniform coating coverage.

INTRODUCTION

Due to their large surface area to volume ratios, adhesion and friction are critical issues for microactuators which contain contacting surfaces in relative motion [1-4]. High static friction is known to contribute to wear and can cause device seizure, and kinetic friction consumes a significant portion of the motive torque [1, 2, 3, 4]. Investigations into the failure modes of electrostatic microengines, for example, indicate that the usual path to failure involves sticking between rubbing surfaces [miller]. In order to operate microactuators with sliding surfaces in high-reliability, long life applications, a robust lubrication scheme which affords precise control of the friction forces is needed.

In microelectromechanical systems (MEMS), contacting surfaces are lightly loaded (≈μN), placing friction in a regime where the contribution from adhesion outweighs those from asperity deformation and ploughing [5,6]. Between oxide-coated surfaces, this adhesion arises from water capillary attractions and can exceed the actuation force. For this reason, Lim and coworkers found the coefficient of static friction between LPCVD polysilicon films to be greater than one– μ_s = 4.9 ± 1.2 [1]. Several experiments have been done to determine a range for kinetic coefficient of friction μ_k for oxide-coated polysilicon contacting surfaces in micromotors. Bart *et al.* reported a μ_k range of 0.26-0.4, and similar ranges have been reported for polysilicon rubbing against silicon [3,13,14].

Low surface energy organic films may be deposited on the contacting surfaces in microactuators to serve as boundary lubricants [bhu]. One possibility that has been investigated is self-assembled monolayers (SAMs) formed from alkyltrichlorosilane precursors [alley, deng, hous]. These organic molecules covalently bond to oxide surfaces and each other through siloxane linkages (Si–O–Si) to give a close-packed monolayer. It has been shown that hydrocarbon and fluorocarbon SAMs give adhesion reductions in polysilicon surface-micromachined test structures of over three orders of magnitude [7-9]. With thicknesses of 1-2 nm, these conformal coatings do not effect bulk material properties significantly, and are therefore well-suited to MEMS [henc]. In addition, alkylsiloxane SAMs have shown exceptional solvent and chemical resistance, good wear and durability properties and stability at the elevated temperatures encountered in MEMS packaging processes [7].

Tribological studies on SAM-coated surfaces have been conducted at the nanoscale using atomic force microscopy (AFM) on smooth surfaces such as silicon (100) and mica [10]. The difficulty in applying results from these types of frictional studies to surface-micromachined devices is that the real area of contact between the relatively rough polysilicon surfaces in MEMS is not easily known. In addition, variability in the topography of LPCVD films makes standardization of surface phenomena of adhesion and friction difficult. At the macroscale, measurements of friction coefficients on SAM-lubricated and oxide-coated Si(100) have been taken using conventional tribometers [10,11]. In these experiments, however, the contact pressure is typically on the order of mN, and adhesion from meniscus formation is no longer significant.

We have fabricated two surface micromachined friction test structures to study friction between laterally sliding polysilicon surfaces as well as vertical sidewalls. In this paper, we present static and dynamic friction coefficients between polysilicon contacts coated with OTS and FDTS SAMs, as well as oxide for

reference. In addition, the wear between the rubbing surfaces in the sidewall device is examined using SEM.

EXPERIMENTAL

Lateral Friction Test Structure. Fig. 1 shows SEM micrographs of the lateral friction test structure after the design of Lim *et al.* [1]. A shuttle with 10×10×1 μm^3 bumpers on its underside is maintained 2 μm above the ground plane by a 200 μm long folded beam suspension. When an electrostatic normal force is exerted on the shuttle, the bumpers land on an electrically separate, grounded polysilicon surface, thereby determining the frictional contact area. The electrostatic comb drive attached to the shuttle is used to determine the spring constant of the folded beam suspension.

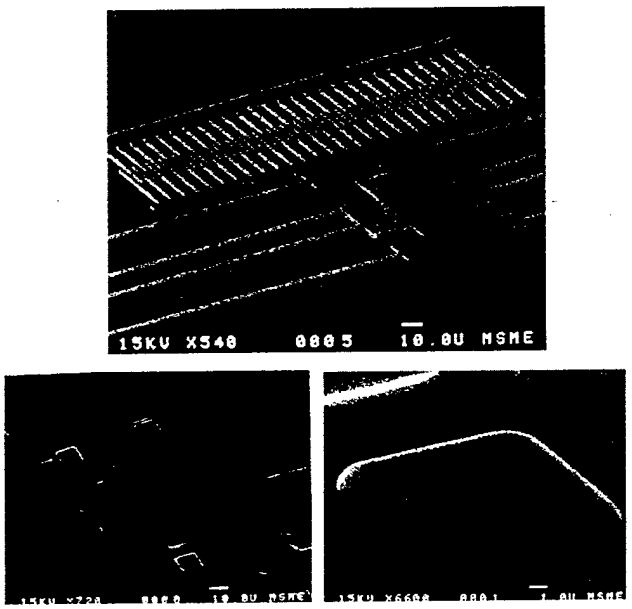

Figure 1. SEM micrographs of a) the lateral friction testing microstructure, consisting of a spring-suspended shuttle attached to an electrostatic comb drive used for spring characterization, b) the underside of the shuttle, and c) a close-up of a 10×10 μm bumper.

These test structures were fabricated in a 4-mask process. The polysilicon film deposition conditions are as follows: 590°C for the ground plane, 585°C for the structural layer, 500 mtorr, and 3.2×10^{-3} mole fraction PH_3 in SiH_4. The 1 μm deep bumper molds are defined in the sacrificial oxide layer using a timed BHF wet etch. To assess frictional dependence on contact area, microstructures with varying numbers of bumpers and total bumper surface area were fabricated. A Topometrix atomic force microscope was used to image the contacting surfaces and study their textures.

Sidewall Friction Test Structure. The sidewall device, shown in Fig. 2, is fabricated from four layers of polysilicon– one electrical and three structural layers. The device is driven by two electrostatic comb drives capable of providing force in both the pushing and pulling directions and with a maximum force output of approximately 10 μN. In the sidewall device, the contacting surfaces are the vertical faces of a moveable, rectangular cross-section beam and a fixed vertical post. The beam has been measured as 2.5 μm thick and 1.8 μm wide using a calibrated SEM for the horizontal measurements and a confocal optical interferometer for the vertical measurements. The post, shown in Fig. 3, has an overall height of 6 μm and is fabricated by the deposition of polysilicon into a 4 μm-deep hole etched through a sacrificial oxide layer to the substrate. The post sits on a grounded electrical polysilicon layer integral with the ground plane of the comb drives.

The beam is brought into contact with the post by applying a voltage to the right-side comb drive, as shown in Fig. 2. The beam is then reciprocated against the post using the bottom comb drive. The contacting geometry is that of a cylinder on a flat since the post has a rounded end with a 2 μm radius. Using a rounded contact geometry ensures that the contact area will remain constant as the beam tilts during movement. Testing was conducted in ambient air.

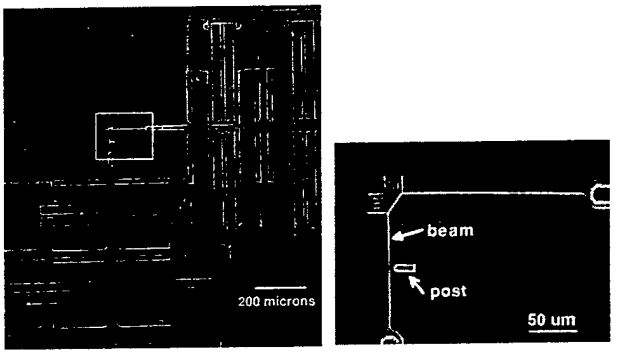

Figure 2. a) An SEM overview of the sidewall device used to measure dynamic friction coefficients. b) A close-up of the structure shown in a) showing the contacting elements.

SAM Coating Process. The structures were released in concentrated HF and then coated with SAMs. The procedure for SAM-coating microstructures is shown in Table 1 [7]. The iso-octane, hexadecane, and chloroform used in the SAM coating are anhydrous (Aldrich), and the remaining chemicals are standard solvent grade. The OTS SAM solution is 0.5 mM of octadecyltrichlorosilane ($CH_3(CH_2)_{17}SiCl_3$, Aldrich, 95% purity) in a 4:1 vol. mixture of hexadecane and chloroform. This solution was prepared and used under a fume hood. The fluorinated SAM solution, 1 mM FDTS ($CF_3(CF_2)_8(CH_2)_2SiCl_3$, PCR Chemicals, 98% purity) in iso-octane (Aldrich), was mixed and used in a N_2-filled drybox to prevent bulk polymerization caused by its highly water-sensitive headgroup. The oxide-coated microstructures used as a benchmark for the friction studies were released using supercritical CO_2 drying following the H_2O_2 reoxidation.

Contact angle measurements were taken with a Ramé-Hart goniometer with water and hexadecane as test liquids. Secondary mass ion spectroscopy (SIMS) was used to verify that the coverage of the SAM coatings was the same on both types of devices.

Table 1. SAM coating procedure for polysilicon microstructures. Solvent changes are accomplished by dilution rinses for the water soluble steps, and by quickly moving the wafer pieces to the next solvent for the organic solvent changes. The duration of each rinse step is ten minutes and the chips were immersed in H_2O_2 and the SAM solution for 15 minutes.

1. Sacrificial Oxide Etch	HF
2. Surface Oxidation	H_2O rinse, H_2O_2 soak, H_2O rinse
3. Bulk Water Removal	IPA rinse (2), Iso-octane rinse (2)
4. SAM Formation	SAM solution
5. Excess Precursor Removal and Dry	Iso-octane rinse (2), IPA rinse (2), H_2O rinse

Lateral Friction Testing Procedure. The testing procedure for the lateral friction testing microstructure is taken from [1]. First, the spring-suspended shuttle is laterally displaced a distance of Δx_1 using a tungsten probe tip or the electrostatic comb drive. Then, the shuttle's bumpers are electrostatically brought into contact with the grounded landing pad by applying a voltage to the underlying electrode (50 and 20V for SAM- and oxide-coated contacts, respectively). When the lateral force is removed, static friction between the contacting surfaces maintains the displacement. The electrostatic clamping force is decreased slowly until the lateral suspension force can overcome the static frictional force, and the shuttle begins to move towards its equilibrium position. The shuttle slides a certain distance and stops at a residual displacement Δx_2. The coefficient of static friction, μ_s, is calculated as follows.

In eq. (1), F_t *and* F_n are the normal and tangential forces exerted on the shuttle at the point of slippage. F_n is composed of the electrostatic clamping force minus the spring suspension's restoring force in the z-direction, and can be calculated according to eq. (2), where α_z is a correction factor to account for fringing effects, l and w are the length and width of the underlying electrode, z is the gap distance, ε_o is the permittivity of air and V_s and V_p are the potentials at which the shuttle begins to slip and where it can overcome the spring's z-restoring force, respectively.

$$F_n = \frac{\alpha_z \varepsilon_0 wl(V_s^2 - V_p^2)}{2z^2} \tag{2}$$

The lateral spring constant, k_x, used to calculate F_t is computed empirically by resonating the electrostatic comb drive and using Rayleigh's method [1,17]. With dimensions and masses substituted in, eq. 1 is written as follows, where f is the resonant frequency of the spring suspension:

$$\mu_s = \frac{0.2 f^2 \Delta x}{(V_s^2 - V_p^2)} \tag{3}$$

The difference in the shuttle's potential energy between its starting and stopping position is due to dissipation to kinetic friction. Therefore, μ_k can be derived from an energy balance, and is given as follows:

$$\mu_k = \frac{1}{2}\mu_s\left(1 + \frac{\Delta x_2}{\Delta x_1}\right) \tag{4}$$

Testing is done in air ($RH \approx$ 40-50%) at room temperature. For each test structure, f, Δx_1, Δx_2, V_s and V_p are measured and μ_s and μ_k are computed. The reported data is taken from chips from one wafer. For impact tests, the shuttle's bumpers are repeatedly brought into contact with the grounded landed pad using square waves with 30 V amplitude. Both OTS and FDTS SAM-coated devices are subject to 1 million impacts at an apparent contact pressure of 15 kPa. Coefficients of friction are monitored periodically.

Sidewall Friction Testing Procedure. For the sidewall device, the friction force is measured by bringing the beam and post into contact, causing the beam to reciprocate against the post, and then measuring the amplitude of the resulting motion. This amplitude is compared to the amplitude resulting when there is no contact between the beam and post. The measured deflections are related to the applied force by applying a voltage to the comb drive and measuring the resulting deflection of the beam perpendicular to the motion. The force acting on the deflecting beam is given by

$$P = \frac{3EI\delta}{L^3} = k\delta \tag{5}$$

where P is the applied force, δ is the deflection of the beam, L is the length of the beam, E is Young's modulus, and I is the moment of inertia given by $bh^3/12$, with b and h as the height and width of the beam, respectively. A value of 160 GPa has been used for Young's modulus.

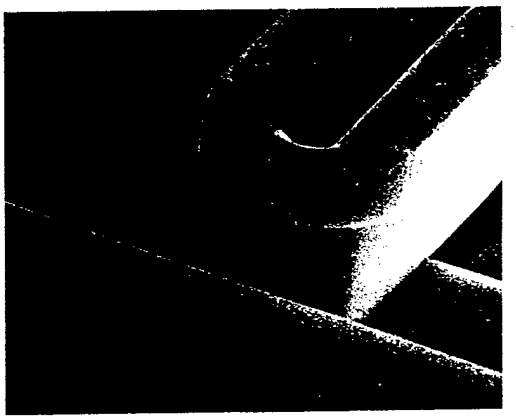

Figure 3. SEM (6 kX magnification) of contacting elements in the sidewall device. The beam rubs on the lower vertical sidewall of the post, and the cap on the post prevents the beam from sliding off.

The forces acting on the beam are the comb drive and the opposing forces of the internal comb drive springs and the frictional force when the surfaces are in contact. The force supplied by the comb drive is due to the electrostatic force minus the frictional losses internal to the comb drive. The normal force on the post is calibrated by measuring the deflection of the beam in the opposite direction, away from the post, as a function of the applied comb drive voltage. A force of 2.8 μN is required to bring the beam into contact with the post. Additional force exerted by the comb drive results in a normal force applied on the post. The magnitude of the normal force is calculated from an elastic model of the structure.

The friction force between the beam and post, f_d is given by [23]

$$f_d = F_c - (k_c + k_b)\delta = (k_c + k_b)(\delta_0 - \delta) \tag{6}$$

where F_c is force supplied by the comb drive, δ_0 is the amplitude of the displacement when there is no contact, δ is the amplitude of the displacement when the surfaces are in contact, and k_c and

k_b are the spring constants for the comb drive springs and the beam, respectively. The spring constants for the beams were calculated from the measured dimensions of the beams and equation (5). The spring constant for the shorter beam that rubs against the post is 0.37 N/m and 0.087 N/m for the perpendicular beam. The spring constant for the comb drive springs was calculated from the slope of the curve for the displacement versus the square of the comb drive voltage and found to be 0.071 N/m. This value is in agreement with that found by Miller et al [24] in an independent measurement using the resonant frequency of these comb drives.

For the experiments, the oscillating comb drive was driven with 44 V amplitude, 100 Hz square waves. A normal force of 1.3 μN was applied between the beam and the post to give a Hertzian contact pressure of 84 MPa. The actual pressure at contacting asperities was larger than this value due to the roughness of the etched sidewall surfaces. The actual roughness of the surfaces could not be determined since the vertical surfaces are inaccessible to AFM measurement.

The amplitude of the device motion was measured by capturing images using a strobe light synchronized with the drive signals. Positions of the device in images taken at 0 degrees and 180 degrees with respect to the drive signals show the maximum displacements of the device in both directions.

RESULTS

Lateral Friction. Atomic force microscopy of the ground plane polysilicon gives an rms roughness of 5 nm (Fig. 3). Contact angle measurements with water (≈110° for both SAMs) and hexadecane (38° for OTS, 68° for FDTS) confirm that well-packed SAMs were formed [7,8].

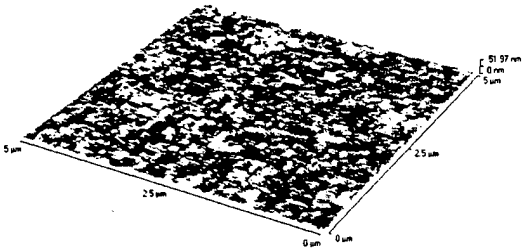

Figure 4. 5X5 μm² AFM image of polysilicon surface from the ground plane. The maximum height is 52 nm and rms roughness is 3 nm.

The normal and tangential forces at the onset of shuttle slippage, μ_s and μ_k values are given in Table 3. Data from test structures with different total bumper areas is shown in Table 4. For all three coatings, stick-slip motion was observed for a 1 V/s decrease of the clamping force, while motion appeared continuous for faster ramp-down rates (5 V/s). The SAM-coated structures also showed continuous motion at the 1 V/s ramp-down rate.

Table 3. Average normal and tangential forces (F_n and F_t) (RH = 50%). The total bumper area is 300 μm² and the shuttle displacement is 12 μm.

	F_n (μN)	F_t (μN)	μ_s	μ_k
Oxide	0.48	1.1	2.0 ± 0.8	-
OTS	10.0	1.4	0.11 ± 0.02	0.08 ± 0.01
FDTS	9.1	0.76	0.09 ± 0.01	0.08 ± 0.01

Table 4. Static coefficient of friction data taken from test structures with total bumper areas of 144 and 300 μm².

	μ_s (A = 144 μm²)	μ_s (A = 300 μm²)
Oxide	2.3 ± 0.8	2.0 ± 0.8
OTS	0.11 ± 0.01	0.11 ± 0.02
FDTS	0.10 ± 0.007	0.09 ± 0.01

Sidewall Friction. A plot of the sidewall friction coefficient as a function of the number of wear cycles is shown in Fig. 5. The initial friction coefficient is 0.02 but rises rapidly after 6000 wear cycles to an average value of 0.23. After 3.7×10^5 cycles, stick-slip motion predominates, indicated in Fig. 5 by the oscillation between high and low friction coefficient values. Friction coefficient values of ~0.8 result when the force of the comb drive is insufficient to move the structure. In this case, the plotted value of 0.8 is a lower bound to the actual friction coefficient. The test was continued for 2.3×10^7 cycles with the number of stick-slip events reduced after 5 million cycles. and the friction coefficient slowly rises to 0.28.

After testing the contacting surfaces were imaged by SEM and shown in Fig. 6. A buildup of material, presumably wear debris, can be seen on the surface of the post. The surface of the beam shows a horizontal scratch and agglomerations of wear particles, each particle ~10 nm in size. SEM photos of unworn structures do no show evidence of particles or scratches. [25]

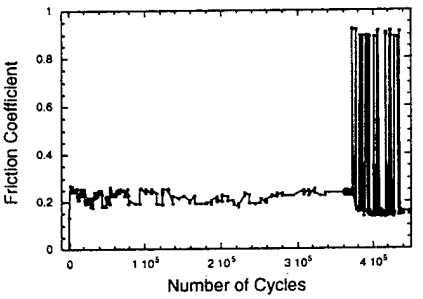

Figure 5. The friction coefficient measured by the sidewall device during sliding friction. The large friction values intermittently measured after 3.7×10^5 cycles are due to sticking of the surfaces.

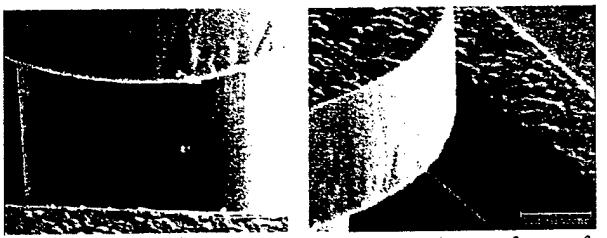

Figure 6. SEM examination of the contacting surfaces of the sidewall device after 2×10^7 wear cycles shows a buildup of wear debris on the post and a horizontal scratch on the beam.

Impact Behavior. OTS and FDTS SAM-coated lateral friction testing devices subject to 1 million impact cycles at an apparent contact pressure of 15 kPa showed no degradation in μ_s and μ_k values.

DISCUSSION

Lateral Friction. Large differences in the static friction force are seen between structures coated with SAMs and SiO_2. The experiments performed on the lateral friction test structures give μ_s of 0.11 ± 0.02 and 0.09 ± 0.01 for OTS and FDTS films, respectively. These values are approximately 20 times lower than μ_s for the standard oxide coating, 2.1 ± 0.8. The results in Table 4 indicate that in this testing situation, these coefficients do not depend on apparent contact area, as expected from Amonton's law [1,18,19].

This dramatic reduction in μ_s can be attributed to the lack of capillary attractions between the hydrophobic SAM surfaces since friction between two surfaces arises from localized adhesion at the points of real contact. Tests on cantilever beam arrays on the same chip support this– the apparent adhesive energy between the polysilicon surfaces is reduced by four orders of magnitude due to FDTS SAM films through the elimination of capillary condensation [7].

The dynamic coefficients of friction (μ_k = 0.08 ± 0.02 for both SAMs) coincide well with literature results taken at the macroscale with pin-on-disc tribometers. Published values of μ_k for OTS SAM-coated Si (100) range from 0.07 to 0.12 [11]. For the fluorinated monolayers, DePalma and Tillman [depa] report higher friction coefficients (μ_k of 0.16) despite their lower surface energies [chau]. This has been attributed to greater adhesion hysteresis between the fluorinated films caused by the less dense packing of the fluoroalkyl chains. This difference in μ_k was not observed in this study, possibly since the OTS films are of a slightly lower quality than those discussed in (contact angle with hexadecane of 38° versus 45-48°). This may be due to the absence of carbon tetrachloride as a co-solvent in the OTS SAM solution in this work [7].

Using similar test structures, Lim and coworkers reported higher μ_s values of 4.9 ± 1.2 for oxide-coated polysilicon contacts. The difference in μ_s may be caused by the drying technique used, i.e., methanol rinse followed by air drying by Lim, *et al.* versus supercritical drying with ultra pure CO_2 in this paper. The high standard deviations in μ_{oxide} data given here as well as by Lim, *et al.* can be explained by considering that high surface energy oxide films favor the adsorption of polar contaminants from the ambient atmosphere, resulting in a highly variable surface layer. In contrast, low standard deviations in the friction data for the SAM films indicate uniform monolayer coverage.

The stick-slip motion observed for all three surface treatments can be due to $\mu_s > \mu_k$ [10]. With the SAM coatings, however, continuous sliding was sometimes seen, indicating $\mu_s \approx \mu_k$.

Sidewall Friction. Sidewall Friction. The friction coefficient measured at the beginning of the test is comparable with that measured by the lateral measurement although the contact pressure and the surface roughness differ in the two experiments. The contact pressure in the sidewall measurements was a factor of 1000 higher than in the lateral measurements, neglecting the roughness of the sidewall surface.

The rise in the friction coefficient during testing is due, at least in part, to the accumulation of wear debris. Evidence of the wear debris is seen in the SEM photos taken after testing.

Impact Behavior. After 1 million impacts at an apparent pressure of 15 kPa, neither SAM film shows degradation in friction coefficients.

CONCLUSIONS AND FUTURE WORK

The results presented here show that nanometer thick SAMs can serve as effective boundary lubricants of microactuators. The SAM μ_k values are similar to that derived from Teflon-coated microengines (0.07) [snie], and lower to those reported for inorganic films under similar apparent pressures [beer].

Also, since SAM coatings are conformal, they offer advantages over thin polymer films deposited in line-of-sight plasma processes.

Future testing of friction measurements of sidewall surfaces will involve testing of OTS coatings and an exploration of the behavior at lower contact pressures. In particular, it would be of interest to collect more data points in the initial, low friction regime.

Acknowledgments

This research has been supported by Sandia National Laboratories. The work done at Sandia National Laboratories is supported by the United States Department of Energy under Contract DE-AC04-94AL85000. The authors acknowledge additional support from the National Science Foundation in the form of a graduate fellowship (US) and a young investigator award (RM). Additional support from The Arnold and Mable Beckman Foundation in form of a young investigator award (RM) is gratefully acknowledged. The authors would like to thank Dr. Michael Houston for his work in fabricating the test structures as well as the Berkeley Microfabrication Staff for their assistance. In addition, the authors would like to thank the staff of the Sandia National Laboratories Microelectronics Development Laboratory for fabricating the sidewall device.

References

1. Lim, M.G., Chang, J.C., Schultz, D.P., Howe, R.T., and White, R.M., *Proceed. IEEE MEMS Workshop,* Napa Valley, CA, U.S.A., 1990, pp. 82-88; Lim, M.: Masters Thesis, University of California at Berkeley, Berkeley CA, 1990.

2. Deng, K., Collins, R.J., Mehregany, N., and Sukkenik, C.N., *Proceed. IEE MEMS Workshop,* Amsterdam, the Netherlands, 1995, pp. 368-375; Deng, K., Ph.D.: Thesis, Case Western Reserve University, Cleveland OH, 1994.

3. Zarrad, H. et al.: *Sensors and Actuators A*, **46/47**, 598-600 (1995).

4. Garcia, E.J. and Sniegowski, J.J.: *Journal of Sensors and Actuators*, **A48**, 203 (1995).

5. Bhushan, B.: *Tribology and Mechanics of Magnetic Storage Devices* (Springer, New York, 1990).

6. Komvopoulos, K.: Personal Communication.

7. Srinivasan, U., Houston, M.R., Howe, R.T. and Maboudian, R.: *Proceedings of the 1997 International*

Conference on Solid State Sensors and Actuators, Chicago IL, USA 1399-1402 (1997).

8. Ulman, A.: *Introduction to Ultra-Thin Organic Films: From Langmuir Blodgett to Self-Assembly*, Academic Press, San Diego, CA, 1991.

9. Houston, M.R., Maboudian, R. and Howe, R.T.: *Proc. IEEE Solid-State Sensor Actuator Workshop,*

Hilton Head, SC, USA (1996).

10. Bhushan, B., Israelachvili, J. and Landman, U.: *Nature*, **374**, 607-616 (1995).

11. Cléchet, P., Martelet, C., Belin, M., Zarrad, H., Jaffrezic-Renault, N. and Fayeulle, S.: *Sensors and Actuators A,* **44,** 77 (1994).

12. Deng, K., Ko, W.H. and Michal, G.M.: *Proceedings of the 1991 International Conference on Solid State Sensors and Actuators*, San Francisco, CA, USA 213-216 (1991).

13. Tai, Y-C. and Muller, R.S.: *Sensors and Actuators A*, **21-23**, 180-183 (1990).

14. Gabriel, K.J., Behi, F., Mahadevan, R. and Mehregany, M.: *Sensors and Actuators A*, **21-23**, 184-188

(1990).

15. Smith, B.K., Sniegowski, J.J. and LaVigne, G.: *Proceedings of the 1997 International Conference on*

Solid State Sensors and Actuators, Chicago IL, USA 245-248 (1997).

16. Mastrangelo, C.H. and Hsu, C.H.: *Proc. IEEE Solid-State Sensor Actuator Workshop,* Hilton Head, SC, USA, 208 (1992).

17. Tang, W.: Ph.D. Thesis, University of California at Berkeley, Berkeley CA, 1990.

18. Bowden, F.P. and Tabor, D.: *Friction and Lubrication,* Methuen & Co., 1967.

19. Rabinowicz, E.: *Friction and Wear of Materials*, John Wiley & Sons, 1965.

20. Srinivasan, U., Howe, R.T. and Maboudian, R.: work in progress.

21. M. K. Chaudhury and M. J. Owen, "Adhesion Hysteresis and Friction", *Langmuir, 9*, 29 (1993).

22. V. DePalma and N. Tillman, "Friction and Wear of Self-Assembled Trichlorosilane Monolayer Films on Silicon", *Langmuir, 5*, 868 (1989).

23. D.C. Senft and M.T. Dugger, "Friction and wear in surface micromachined tribological test devices", SPIE Proceedings Vol. 3224, p. 31-38.

24. S. L. Miller, J. J. Sniegowski, G. LaVigne, and P. J. McWhorter, "Friction in surface micromachined microengines", *Proc. SPIE Smart Electronics and MEMS* Vol. 2722, pp. 197-204, San Diego, 1996.

25. D.M. Tanner, W.M. Miller, W.P. Eaton, et al, "The Effect of Frequency on the Lifetime of a Surface Micromachined Microengine Driving a Load.", Proceedings of the International Reliability Physics Symposium, Reno, NV, 1998.

DISCLAIMER

Report Number (14) SAND--98-0848C
CONF-980638--

Publ. Date (11) 199806

Sponsor Code (18) DOE/DP; NSF; 045, XF

UC Category (19) UC-700; UC-000; UC-000, DOE/ER

DOE